Magnetic ground-state of the highly one-dimensional ferromagnetic chain compounds $M(\mathrm{NCS})_2(\mathrm{thiourea})_2$; M = Ni, Co - Supplemental information.

S. P. M. Curley,[1] R. Scatena,[2,3] R. C. Williams,[1] P. A. Goddard,[1,*] P. Macchi,[4,5,3] T. J. Hicken,[6] T. Lancaster,[6] F. Xiao,[7] S. J. Blundell,[8] V. Zapf,[9] J. C. Eckert,[10] E. H. Krenkel,[10] J. A. Villa,[11] M. L. Rhodehouse,[11] and J. L. Manson[11,†]

[1] *Department of Physics, University of Warwick, Gibbert Hill Road, Coventry, CV4 7AL, UK*
[2] *Department of Physics, Clarendon Laboratory, University of Oxford, Parks Rd., Oxford, OX1 3PU, United Kingdom*
[3] *Department of Chemistry and Biochemistry, University of Bern, 3012 Bern, Switzerland*
[4] *Department of Chemistry, Materials, and Chemical Engineering, Polytechnic of Milan, Milan 20131, Italy*
[5] *Istituto Italiano di Tecnologia, Center for Nano Science and Technology CNST@polimi, Milan 20133, Italy*
[6] *Durham University, Department of Physics, South Road, Durham, DH1 3LE, United Kingdom*
[7] *Laboratory for Neutron Scattering and Imaging, Paul Scherrer Institut, CH-5232 Villigen PSI, Switzerland*
[8] *Department of Physics, Clarendon Laboratory, University of Oxford, Parks Road, Oxford, OX1 3PU, United Kingdom*
[9] *National High Magnetic Field Laboratory, Materials Physics and Applications Division, Los Alamos National Laboratory, Los Alamos, New Mexico 87545, USA*
[10] *Physics Department, Harvey Mudd College, Claremont, CA, United States*
[11] *Department of Chemistry and Biochemistry, Eastern Washington University, Cheney, Washington 99004, USA*

EXPERIMENTAL DETAILS

Synthesis

All chemical reagents were obtained from commercial sources and used as received. All reactions were performed in 50 ml glass beakers. For $\mathrm{Ni(NCS)_2(thiourea)_2}$, an aqueous solution of $\mathrm{NiCl_2}$ (0.3018g, 1.262 mmol) was slowly added to an aqueous solution of $\mathrm{NH_4NCS}$ (0.2113g, 2.7764 mmol) and thiourea (0.1918g, 2.524 mmol) to afford a clear green solution. When allowed to slowly evaporate at room temperature, X-ray quality, dark green, fine, needle-like crystals were recovered. For $\mathrm{Co(NCS)_2(thiourea)_2}$, an aqueous solution of $\mathrm{CoCl_2}$ (0.29996g, 1.2607 mmol) was slowly added to an aqueous solution of $\mathrm{NH_4NCS}$ (0.2111g, 2.7737 mmol) and thiourea (0.1919g, 2.5210 mmol) to afford a slightly cloudy, pink-red solution. When allowed to slowly evaporate at room temperature, X-ray quality, red-brown, large, needle-like crystals were recovered.

Muon Spin Relaxation

In a positive muon spin relaxation (μ^+SR) experiment, positive spin-polarised muons are implanted in a sample where they interact with the local magnetic field. Static magnetic order will typically cause coherent precession of the muon-spin with angular frequency $\omega_\mu = \gamma_\mu B$, where γ_μ is the muon gyromagnetic ratio and B is the local field at the muon site, which is a sum of the internal field arising due to the spin configuration, and the external field $\mu_0 H$. Alternatively, if the system is dominated by dynamic magnetic effects, the muon-polarisation will typically decay exponentially with relaxation rate $\lambda = 2\Delta^2\tau$, where Δ is the width of the field at the muon site and τ is the correlation time of the local field.

After, on average, 2.2 μs, the muon decays into a positron and two neutrinos, where the positron is preferentially emitted along the direction of muon-spin polarisation at the time of decay. By detecting these positrons one can calculate a quantity directly proportional to the muon-spin polarisation, known as the asymmetry,

$$A(t) = \frac{N_\mathrm{F}(t) - \alpha N_\mathrm{B}(t)}{N_\mathrm{F}(t) + \alpha N_\mathrm{B}(t)}, \tag{1}$$

where $N_{\mathrm{F,B}}(t)$ are the number of muons detected in the detectors forward and backward of the initial muon-spin polarisation respectively, and α is an experimental efficiency factor.

Zero field (ZF)-μ^+SR measurements on two polycrystalline compounds, $M(\mathrm{NCS})_2(\mathrm{thiourea})_2$ where M = Ni or Co, were made using the GPS instrument at Swiss Muon Source (SμS), Paul Scherrer Institut (PSI). The samples were packed in a silver foil packet (thickness 25 μm) and mounted on the end of a fork in a ^{4}He Quantum Cryostat. Data analysis was performed using both WiMDA [1] and our own software developed for global fitting.

Heat capacity

Heat capacity measurements were made on a Quantum Design PPMS instrument. Plate-like single-crystals were available for $\mathrm{Co(NCS)_2(thiourea)_2}$, whilst polycrystalline

powder samples of $Ni(NCS)_2(thiourea)_2$ were pressed into pellets. The samples were mounted onto the sample stage with a small amount of Apiezon vacuum M-grease to provide good thermal contact between the sample and sample platform. Addenda measurements were performed to correct for the heat capacity of the sample platform and M-grease. The mounted sample initially sits in thermal equilibrium with the platform. A small heat pulse is then applied and the time taken for the system to relax back to thermal equilibrium monitored. The heat capacity can then be extracted by fitting the resultant relaxation curve [2].

Magnetometry

Magnetometry measurements were performed using a Quantum Design MPMS-7XL SQUID magnetometer. $Ni(NCS)_2(thiourea)_2$ was crushed to a fine powder and mixed with Vaseline to mitigate grain reorientation in the applied field. The Vaseline-sample mix was mounted within a low-magnetic-background gelatin capsule. A plate-shaped single-crystal of $Co(NCS)_2(thiourea)_2$ was mounted on a low-magnetic-background Teflon sample holder in order to measure along all multiple axes of the single-crystal. Both were then placed inside a plastic drinking straw to be measured within the MPMS sample chamber. Temperature sweeps from $1.8 \leq T \leq 300$ K were completed on both compounds. Field sweeps up to $\mu_0 H = 7$ T were completed for $Ni(NCS)_2(thiourea)_2$. For $Co(NCS)_2(thiourea)_2$, application of sizable magnetic fields perpendicular to the Co(II) Ising-axis regularly shattered or re-orientated the samples, regardless of the method used to affix them.

Charge and spin density

Single-crystal X-ray measurements were performed on $Co(NCS)_2(thiourea)_2$ and $Ni(NCS)_2(thiourea)_2$ using an Oxford Diffraction SuperNova area-detector diffractometer. An Al-filter was used to reduce the number of low-energy photons contaminating the incident Mo K_α radiation (λ =0.71073 Å) [3]. Single-crystals were adhered to a glass fibre and low-temperatures achieved using an Oxford Cryostream flow cryostat. Extensive high-resolution data collections ($d_{\min}$ = 0.50 Å) were performed at 100.0(2) K for $Co(NCS)_2$ $(thiourea)_2$; $Ni(NCS)_2$ $(thiourea)_2$ data was collected at 173.0(2) K, up to a resolution of 0.70 Å. Due to $Ni(NCS)_2(thiourea)_2$ single-crystals being irremediably affected by twinning, high quality X-ray data collection, required for charge density modelling, could only be performed for $Ni(NCS)_2(thiourea)_2$. Data reductions were performed using CrysAlisPro software [4]. Intensities were analytically corrected for Lorentz, polarisation and absorption effects using the Gaussian method, based on the dimensions of the $Co(NCS)_2(thiourea)_2$ single-crystals. For $Ni(NCS)_2(thiourea)_2$, a semi-empirical correction was applied. The conventional structural refinements were carried out with SHELXL [5].

For charge density analysis of $Co(NCS)_2(thiourea)_2$, the atomic and thermal parameters obtained from spherical refinement were used as a starting point for the Multipolar Model refinement within the Hansen-Coppens formalism [6] for electron charge density determination. Calculations were performed using XD2016 [7]. All multipoles of non-hydrogens atoms were refined up to the hexadodecapole. κ and κ' parameters were also freely refined except for the S atom where they were constrained to vary equally. Hydrogen atoms were restrained to calculated distances and refined using a riding model. Only the monopole and a dipole oriented in the bond direction were refined for the hydrogens. Both κ and κ' were constrained to 1.3 and 1.2, respectively. Residual density maps show small and rather random discrepancies. Topological properties of the electron density, integrated atomic charges and electrostatic potential were calculated with the XDPROP module of XD software.

Periodic Density Functional Theory (p-DFT) calculations of geometry optimizations and electron density distributions for both compounds were carried out using CRYSTAL14 software [8]. The functional B3LYP was used with basis pob-TZVP [9]. The theoretical electron density was analyzed with the TOPOND module of CRYSTAL14. Computed structure factors were refined with the multipolar model using XD2016 [7].

RESULTS

Muon Spin Relaxation

Spectra measured in the magnetically ordered regime for $Ni(NCS)_2(thiourea)_2$, were fitted with

$$A(t) = \sum_{i=1}^{2} A_i e^{-\lambda_i t} \cos(2\pi\nu_i t + \phi_i) + A_3 e^{-\lambda_3 t} + A_{\mathrm{bsln}} e^{-\lambda_{\mathrm{bsln}} t}, \quad (2)$$

where A_i are the relaxing asymmetry of each component with corresponding relaxation rate λ_i, oscillation frequency ν_i, and the phase ϕ_i. The amplitude A_{bsln} is the baseline asymmetry (accounting for both muons stopping outside of the sample and for those that stop within the sample but only have a component of their spin along the local field direction) which has relaxation rate λ_{bsln}. Each component of the model accounts for muons that stop in different local environments, with the two oscillatory components accounting for muons that stop in two different local magnetic fields that lead to coherent precession, indicative of long range magnetic order.

To account for the spectra measured at $T \lesssim 7$ K, which showed a third frequency at approximately $3\nu_1$, a purely relaxing component was included in the fitting to account for the rapid depolarisation of the initial muon-spin due to this third precession rate. As expected, the relaxation rate of this component λ_3 is large at low temperatures and drops for $T \gtrsim 7$ K. This indicates a broad transition region, similar to the observation made on $Co(NCS)_2(thiourea)_2$ in the main text.

Above T_N, where oscillations are not resolvable in the spectra, the data are well described by a model comprising of two relaxing components,

$$A(t) = \sum_{i=1}^{2} A_i e^{-\lambda_i t} + A_{\rm bsln} e^{-\lambda_{\rm bsln} t}. \quad (3)$$

The background relaxation rate $\lambda_{\rm bsln}$ was set to be equal to that found from fitting below T_N, and all other parameters were globally refined to be constant over the entire temperature range, except for the small relaxation rate λ_1, which was found to decrease on increasing temperature.

For the ZF-μ^+SR asymmetry spectra measured for $Co(NCS)_2(thiourea)_2$, Eqn. 3 was fitted over the entire temperature range. The background relaxation rate $\lambda_{\rm bsln}$ and the large relaxation rate λ_2 were globally refined over all the datasets to obtain the best fits.

Heat Capacity

Figure S1 shows zero-field heat capacity (C) divided temperature (T) and plotted as a function of T for both compounds. Both C/T datasets show sharp peaks at $T_c = 6.82(5)$ K and 10.5(1) K for the Co(II) and Ni(II) respectively, indicative of long-range ordering. To isolate the low-temperature magnetic contribution to the heat capacity, the high-temperature ($T \gtrsim 30$ K) contribution ($C_{{\rm high}T}$) can be reproduced by a model containing two Einstein and one Debye phonon mode, with the resultant fit subtracted as a background ($C_{\rm mag} = C - C_{{\rm high}T}$) as described in [10]. The black lines in Figure S1 are fits to $C_{{\rm high}T}$, the resultant fit parameters are shown in Table SI. The model used to fit the high-temperature heat capacity is purely phenomenological and is not intended to provide an accurate parameterization of the lattice dynamics.

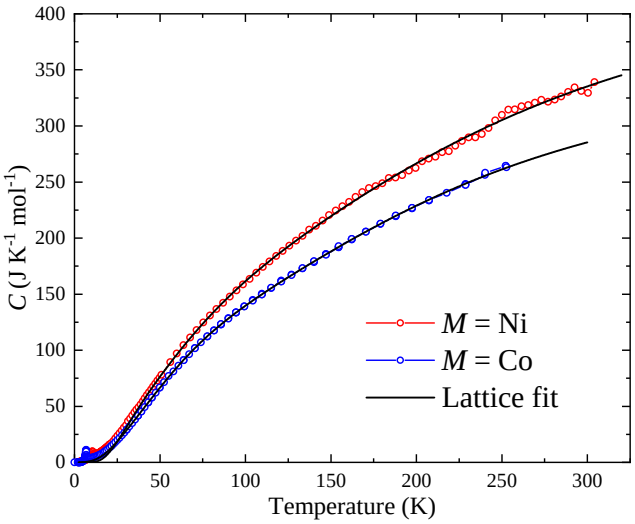

FIG. S1. Heat capacity (C) measured in zero-field and plotted as a function of temperature for Co(NCS)2(thioures)2 and Ni(NCS)2(thiourea)2, solid lines are fits to two Einstein and one Debye mode for the temperature range $T > 30$ K and $T > 37$ K, respectively. Fit parameters are shown in Table SI.

TABLE SI. Fitted high-temperature contribution to the heat capacity for $Co(NCS)_2(thiourea)_2$ and $Ni(NCS)_2(thiourea)_2$. A_i is amplitude of mode i, whilst θ_i is the characteristic temperature of the mode i (i = D, Debye; i = E, Einstein).

Parameter	$Co(NCS)_2(thiourea)_2$	$Ni(NCS)_2(thiourea)_2$
$A_{\rm D}$ (J/K.mol)	94(4)	172(5)
$\theta_{\rm D}$ (K)	172(3)	443(28)
$A_{\rm E_1}$ (J/K.mol)	105(3)	96(8)
$\theta_{\rm E_1}$ (K)	285(7)	126(5)
$A_{\rm E_2}$ (J/K.mol)	172(3)	185(6)
$\theta_{\rm E_2}$ (K)	816(13)	941(46)

For the Co(II) species, the large negative single-ion anisotropy (SIA) term splits the two Kramer doublets such that, at low temperatures, the system can be well approximated by the effective spin-half Ising model. The sharp nature of the peak in $C_{\rm mag}$ rules out strictly 1D behaviour, where spin-spin correlations begin to build up well before T_c, resulting in a broad transition. For a 2D square lattice of Ising-spins with anisotropic exchange interactions (J, J'), the $C_{\rm mag}$ response can be simulated by considering Eq. 4, as derived by Onsager [11, 12], where J and J' obey:

$$\sinh(\frac{2J}{T_c})\sinh(\frac{2J'}{T_c}) = 1 \quad (4)$$

Here, J and J' are the magnetic exchange interactions along two different directions within the 2D lattice. Taking $T_c = 6.82(5)$ K, $C_{\rm mag}(T)$ can be simulated and compared to the measured response for various sets of $\{J, J'\}$ which obey Eq. 4. The simulated curves (solid lines) were then compared to the measured response for Co(NCS)2(thiourea)2 (open squares) with the results shown in Figure S2.

The simulated curves do not capture the data convincingly, leading to the conclusion that $C_{\rm mag}$ cannot be well described by the 2D Ising model. We interpret this result as evidence to support a 3D Ising long range ordering

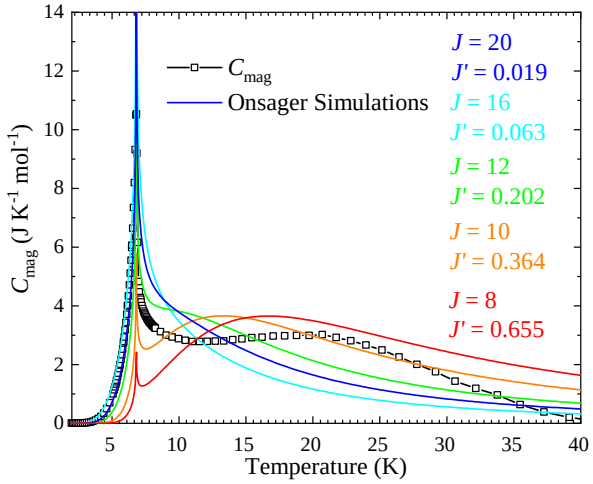

FIG. S2. Magnetic heat-capacity C_{mag} (squares) plotted as a function of temperature T. Simulated $C_{\mathrm{mag}}(T)$ curves (solid lines) are plotted for a selection of exchange values $\{J, J'\}$ which obey the Onsager relation (Eq. 4) for a 2D lattice of Ising spins.

within the Co compound. The two classes of interchain exchange interaction are therefore expected to be comparable in magnitude, and the number of interchain next nearest neighbours expected to be $n' = 4$.

Charge and spin density

Selected structural refinement parameters for single-crystal X-ray refinement of $Co(NCS)_2(thiourea)_2$ and $Ni(NCS)_2(thiourea)_2$ are shown in Table SIV, where the lack of twinning in the Co species allowed high-quality multipolar model (MM) refinement. The MM refinements were used to calculate the electron deformation density maps (Figure 9, main text) by comparing it to that calculated by a simple Independent Atom Model (IAM).

A fractal dimension plot, comparing the residuals of these two methods, shown in Figure S3 reports small and rather random discrepancies. The electron density and its Laplacian at the bond critical point have equivalent values in corresponding M-ligand interactions in these materials, see Table SV.

Topological analysis of the experimental and theoretical electron densities are shown in Table SIII. Periodic Density Functional Theory (p-DFT) calculations of geometry optimizations and electron density distributions for both $Co(NCS)_2(thiourea)_2$ and $Ni(NCS)_2(thiourea)_2$ were carried out by using CRYSTAL14 software [8]. Optimized structural parameters and selected bond lengths are shown in Table SVI. These parameters were then used to calculate values for the magnetic superexchange coupling constants with the results shown in Table SII. The conversion from ΔE to J was done by considering a single J convention in the Hamiltonian, so summations were completed over unique exchange pathways.

TABLE SII. Energy differences (ΔE) and calculated magnetic super-exchange coupling constants (J) between nearest neighbour transition metal-ions along the principle crystallographic axes. Conversion from ΔE to J is done by considering a single J convention. Negative values describe antiferromagnetic interactions.

	$Co(NCS)_2(thiourea)_2$		$Ni(NCS)_2(thiourea)_2$	
Axis	ΔE (K)	J (K)	ΔE (K)	J (K)
a	25.31	4.22	234.38	78.13
b	-0.61	-0.10	-0.34	-0.11
c	-0.51	-0.08	0.20	0.07

TABLE SIII. Quantum theory of atoms in molecules integrated atomic charges for $Co(NCS)_2(thiourea)_2$ and $Ni(NCS)_2(thiourea)_2$ as obtained from multipolar modelling (MM) to experimental structure factor (Exp. MM) and calculated structure factor (Calc. MM), or from periodic-DFT electron density distribution (p-DFT).

	$Co(NCS)_2(thiourea)_2$			$Ni(NCS)_2(thiourea)_2$	
Atomic charges	Exp. MM	Calc. MM	p-DFT	Calc. MM	p-DFT
M	1.233	1.348	1.294	0.905	1.154
		NCS^-			
S(1)	-0.304	-0.192	-0.140	-0.264	0.135
N(1)	-0.757	-0.785	-1.219	-0.583	-1.203
C(1)	0.058	0.153	0.303	0.114	0.307
NCS^-	-1.003	-0.824	-1.056	-0.733	-0.761
		thiourea			
S(2)	-0.110	-0.396	0.144	-0.417	-0.087
N(2)	-1.123	-0.877	-1.093	-0.916	-1.099
N(3)	-1.153	-0.810	-1.102	-0.927	-1.095
C(2)	0.737	0.704	0.683	0.649	0.685
H(2A)	0.535	0.471	0.454	0.473	0.443
H(2B)	0.517	0.351	0.442	0.463	0.455
H(3A)	0.424	0.345	0.447	0.483	0.438
H(3B)	0.572	0.342	0.437	0.476	0.446
thiourea	0.399	0.130	0.412	0.284	0.186

TABLE SIV. Single crystal X-ray data and refinements details for $Co(NCS)_2(thiourea)_2$ and $Ni(NCS)_2(thiourea)_2$.

Compound	$Co(NCS)_2(thiourea)_2$	$Ni(NCS)_2(thiourea)_2$
Formula	$Co_1S_4N_6C_4H_8$	$Ni_1S_4N_6C_4H_8$
M.W. / g·mol^{-1}	327.34	327.10
Temperature / K	100(2)	173(2)
Crystal system	primitive	primitive
Space group	$P\bar{1}$	$P\bar{1}$
a / Å	3.82030(10)	3.7615(2)
b / Å	7.5341(2)	7.5273(5)
c / Å	10.0847(2)	10.0744(7)
α / °	92.065(2)	92.129(5)
β / °	98.230(2)	98.055(5)
γ / °	104.835(2)	104.080(5)
Volume / Å^3	276.896(2)	273.19(3)
Z	1	1
ρ_{calc} / g·cm^{-3}	1.961	1.988
μ / mm^{-1}	2.275	2.513
2θ range /°	4.1 - 90.7	4.1 - 26.2
h index range	-7 / 7	-4 / 4
k index range	-15 / 14	-9 / 9
l index range	-20 / 20	-13 / 13
Collected/unique	40906 / 4662	4059 / 2315
R_{int}	0.040	0.039
R_σ	0.018	0.049
	Spherical atom refinement	
Data/restr./param.	4527/0/71	2315/0/87
GooF on F^2	1.057	1.028
R indexes [I≥2$_\sigma$]	R1 = 0.022	R1 = 0.030
	wR2 = 0.06	wR2 = 0.08
Residuals /eÅ^{-3}	0.75/-0.95	0.64/-0.32
	Multipole model refinement	
Data/restr./param.	4650/0/279	
GooF on F^2	1.069	
R indexes [all data]	R1 = 0.019	
	wR2 = 0.05	
Residuals / eÅ^{-3}	0.63/-0.75	

TABLE SV. Selected bond critical point properties for $Co(NCS)_2(thiourea)_2$ and $Ni(NCS)_2(thiourea)_2$ where M is the transition metal ion Ni(II) or Co(II). ρ_{bcp} and $\bigtriangledown\rho_{bcp}$ are the electron density (e/bohr^3) and its Laplacian (e/bohr^5). ϵ is the dimensionless bond ellipticity.

	$Co(NCS)_2(thiourea)_2$						$Ni(NCS)_2(thiourea)_2$		
	Exp. MM			Calc. MM			Calc. MM		
bond	ρ_{bcp}	$\bigtriangledown\rho_{bcp}$	ϵ	ρ_{bcp}	$\bigtriangledown\rho_{bcp}$	ϵ	ρ_{bcp}	$\bigtriangledown\rho_{bcp}$	ϵ
M—N	0.069(2)	0.348(1)	0.41	0.071	0.341	0.14	0.073	0.343	0.01
M—S	0.031(1)	0.126(0)	0.75	0.035	0.118	0.01	0.038	0.116	0.05
M—S	0.034(1)	0.125(0)	0.30	0.038	0.130	0.02	0.041	0.126	0.05
M—M	0.016(1)	0.046(0)	*1.66*	0.016	0038	*1.94*	-	-	-
				NCS^-					
N(1)-C(1)	0.448(6)	-0.075(10)	0.09	0.454	-0.716	0.01	0.454	-1.009	0.02
C(1)-S(1)	0.255(7)	-0.533(6)	0.10	0.197	0.064	0.06	0.2	-0.247	0.03
				thiourea					
S(2)-C(2)	0.209(6)	-0.357(4)	0.25	0.182	-0.249	0.05	0.182	-0.192	0.07
C(2)-N(2)	0.366(5)	-1.111(8)	0.12	0.342	-0.935	0.10	0.349	-0.814	0.21
C(2)-N(3)	0.354(5)	-1.116(8)	0.11	0.342	-0.899	0.11	0.351	-0.839	0.23

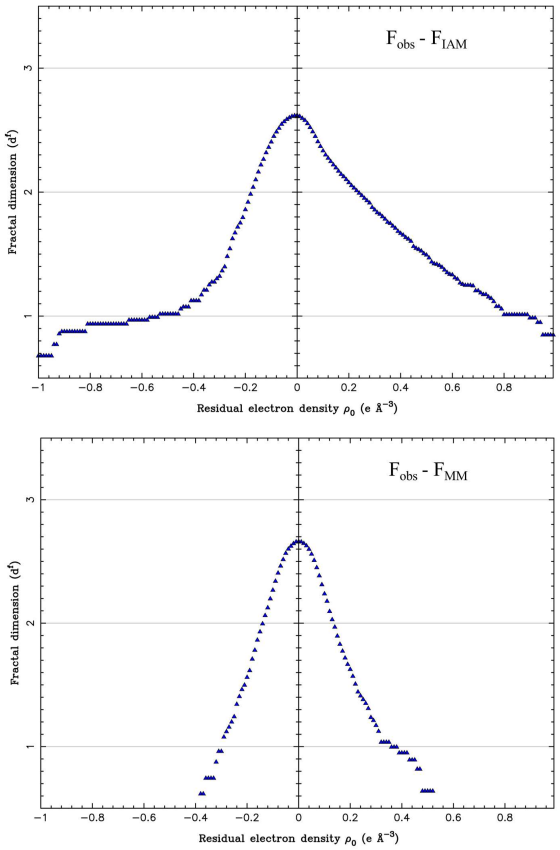

FIG. S3. Fractal dimension plot of residuals for Independent Atom Model (IAM) (upper panel) and Multipole Model (MM) (lower panel) refinements of $Co(NCS)_2(thiourea)_2$ X-ray data.

TABLE SVI. Peridoc-DFT geometry optimizations of $Co(NCS)_2(thiourea)_2$ and $Ni(NCS)_2(thiourea)_2$ where M represents either Ni(II) or Co(II).

Compound	$Co(NCS)_2(thiourea)_2$	$Ni(NCS)_2(thiourea)_2$
Space group	$P\bar{1}$	$P\bar{1}$
a / Å	3.88868	3.83801
b / Å	7.83699	7.60047
c / Å	10.22564	10.18991
α / °	96.04319	92.10032
β / °	98.42657	98.47791
γ / °	108.42653	99.92120
Volume / Å^3	291.884	289.014
	Bond lengths and angles	
M—S / Å	2.567	2.549
M—S / Å	2.605	2.585
M—N / Å	2.052	2.026
M—M / Å	3.889	3.838
M—S—M / °	97.51	96.77
S—M—S / °	82.49	83.23

* p.goddard@warwick.ac.uk
† jmanson@ewu.edu

[1] F. Pratt, Physica B: Condensed Matter **289**, 710 (2000).
[2] J. Lashley, M. Hundley, A. Migliori, J. Sarrao, P. Pagliuso, T. Darling, M. Jaime, J. Cooley, W. Hults, L. Morales, D. Thoma, J. Smith, J. Boerio-Goates, B. Woodfield, G. Stewart, R. Fisher, and N. Phillips, Cryogenics **43**, 369 (2003).
[3] P. Macchi, H.-B. Bürgi, A. S. Chimpri, J. Hauser, and Z. Gál, J. Appl. Crystallogr. **44**, 763 (2011).
[4] "Crysalispro," CrysAlisPRO, Oxford Diffraction /Agilent Technologies UK Ltd, Yarnton, England.
[5] G. M. Sheldrick, Acta Crystallographica Section C **71**, 3 (2015).
[6] N. K. Hansen and P. Coppens, Acta Crystallographica Section A **34**, 909 (1978).
[7] A. Valkov, P. Macchi, L. J. Farrugia, C. Gatti, P. Mallinson, T. Richter, and T. Koritsanszky, "XD2016," (2016).
[8] R. Dovesi, R. Orlando, A. Erba, C. M. Zicovich-Wilson, B. Civalleri, S. Casassa, L. Maschio, M. Ferrabone, M. De La Pierre, P. D'Arco, Y. Noël, M. Causà, M. Rérat, and B. Kirtman, Int. J. Quantum Chem. **114**, 1287 (2014).
[9] M. F. Peintinger, D. V. Oliveira, and T. Bredow, Journal of Computational Chemistry **34**, 451 (2013).
[10] W. J. A. Blackmore, J. Brambleby, T. Lancaster, S. J. Clark, R. D. Johnson, J. Singleton, A. Ozarowski, J. A. Schlueter, Y.-S. Cheng, A. M. Arif, S. Lapidus, F. Xiao, R. C. Williams, S. J. Blundell, M. J. Pearce, M. R. Lees, P. Manuel, D. Y. Villa, J. A. Villa, J. L. Manson, and P. A. Goddard, New J. Phys. **21**, 093025 (2019).
[11] L. Onsager, Phys. Rev. **65**, 117 (1944).
[12] B. M. McCoy and T. T. Wu, *The Two-Dimensional Ising Model* (Harvard University Press, Cambridge MA, 1973).